

Line identification and photometric history of the hot post-AGB star Hen 3-1013 (IRAS 14331-6435)

V. P. Arkhipova¹, M. Parthasarathy^{2*}, N. P. Ikonnikova¹, M. Ishigaki³,
S. Hubrig⁴, G. Sarkar⁵, A. Y. Kniazev^{1,6,7,8}

¹ *Lomonosov Moscow State University, Sternberg Astronomical Institute, 13 Universitetskij prospekt, Moscow 119234, Russia*

² *Indian Institute of Astrophysics, Bangalore 560034, India*

³ *IPMU, The University of Tokyo, Japan*

⁴ *Leibniz Institute for Astrophysics (AIP), Potsdam, Germany*

⁵ *Department of Physics, IIT Kanpur, India*

⁶ *South African Astronomical Observatory, Cape Town, South Africa*

⁷ *Southern African Large Telescope Foundation, Cape Town, South Africa*

⁸ *Special Astrophysical Observatory of RAS, Nizhnij Arkhыз, Karachai-Circassia 369167, Russia*

Accepted 2018. Received 2018; in original form 2018

ABSTRACT

We present a study of the high-resolution optical spectrum for the hot post-asymptotic giant branch (post-AGB) star, Hen 3-1013, identified as the optical counterpart of the infrared source IRAS 14331-6435. For the first time the detailed identifications of the observed absorption and emission features in the wavelength range 3700-9000 Å is carried out. Absorption lines of H I, He I, C I, N I, O I, Ne I, C II, N II, O II, Si II, S II, Ar II, Fe II, Mn II, Cr II, Ti II, Co II, Ni II, S III, Fe III and S IV were detected. From the absorption lines, we derived heliocentric radial velocities of $V_r = -29.6 \pm 0.4$ km s⁻¹. We have identified emission permitted lines of O I, N I, Fe II, Mg II, Si II and Al II. The forbidden lines of [N I], [Fe II], [Cr II] and [Ni II] have been identified also. Analysis of [Ni II] lines in the gaseous shell gives an estimate for the electron density $N_e \sim 10^7$ cm⁻³ and the expansion velocity of the nebula $V_{\text{exp}} = 12$ km s⁻¹. The mean radial velocity as measured from emission features of the envelope is $V_r = -36.0 \pm 0.4$ km s⁻¹. The Balmer lines H α , H β and H γ show P Cyg behaviour which indicate ongoing post-AGB mass-loss. Based on ASAS and ASAS-SN data, we have detected rapid photometric variability in Hen 3-1013 with an amplitude up to 0.2 mag in the V band. The star's low-resolution spectrum underwent no significant changes from 1994 to 2012. Based on archival data, we have traced the photometric history of the star over more than 100 years. No significant changes in the star brightness have been found.

Key words: stars: AGB and post-AGB – stars: atmospheres – stars: early-type – stars: evolution – stars: individual: Hen 3-1013, IRAS 14331-6435.

1 INTRODUCTION

The southern star CPD-64°2939 was identified by [Henize \(1976\)](#) as an H α emission line object and was named Hen 3-1013. [Parthasarathy & Pottasch \(1989\)](#) found it to be an IRAS source with far infrared (IR) colours similar to planetary nebulae (PNe) and suggested that it is in the post-AGB stage of evolution. [Loup et al. \(1990\)](#) detected CO emission in this object and derived an expansion velocity of 15 km s⁻¹. From low resolution optical

spectra [Parthasarathy et al. \(2000a\)](#) find it to be a B3 supergiant with H β in emission and H γ filled in. In 2003 [Gauba & Parthasarathy \(2003\)](#) have estimated the interstellar and circumstellar absorption of Hen 3-1013 on the low resolution *IUE* spectrum from 1150 to 3200 Å. Combining the optical, near and far-IR (*ISO*, *IRAS*) data of IRAS 14331-6435 [Gauba & Parthasarathy \(2004\)](#) have reconstructed its spectral energy distribution (SED) and estimated the dust temperatures, mass loss rates, angular radii of the inner boundary of the dust envelopes and the distances to the star. In *ISO* spectrum these authors have found the amorphous and crystalline silicate features indicating

* E-mail:m-partha@hotmail.com

oxygen-rich circumstellar dust shell of the star. The identical features were observed in oxygen-rich post-AGB stars IRAS 18062+2410 (V886 Her) and IRAS 22023+5249 (LSIII +52 24).

García-Hernández et al. (2002) observed He 3-1013 in 2 μm H₂ survey, have found the emission lines of H₂ molecule and measured the flux ratio of H₂ [$v = 1 \rightarrow 0$ S(1)/2 \rightarrow 1 S(1)] = 8.4 what showed the collisional excitation H₂ in He 3-1013.

Mello et al. (2012) have determined the chemical abundances of He 3-1013 on high resolution spectra obtained on the 2.2-m telescope at La Silla with the FEROS spectrograph. They received the stellar parameters by using of non-LTE model atmospheres BSTAR2006 (Lanz & Hubeny 2007) and estimated the core mass and zero-age mass of the star from evolutionary tracks of post-AGB stars according to Blöcker (1995). The core mass turned out to be $0.70 \pm 0.20 M_{\odot}$ and the metallicity $Z(\text{CNO})=0.016$.

The masses of stars on the post-AGB evolution stage are in the range 0.5-0.8 M_{\odot} . If Hen 3-1013 indeed is related to more massive post-AGB stars ($\sim 0.7 M_{\odot}$) one would expect possible rapid evolution. In this paper, we traced the photometric history of Hen 3-1013 over more than 100 years and analysed the spectroscopic data over the last 20 years to test this assumption.

The optical spectrum of Hen 3-1013 has so far not been studied in sufficient detail. In this paper, we report the results of the high-resolution spectral observations carried out with the aim to study the peculiarities of the spectrum and the details of the velocity field in the atmosphere and envelope of the star.

In Section 2 we briefly describe the spectral observations of Hen 3-1013 and the data reduction process. A detailed analysis of the high-resolution spectrum is presented in Section 3 while the analysis of the low-resolution spectrum is shown in Section 4. A photometric history of Hen 3-1013 is presented in Section 5. We discuss our findings and conclude in Section 6.

2 OBSERVATIONS AND DATA REDUCTION

2.1 High-resolution spectrum

The spectrum of Hen 3-1013 was obtained on April 14, 2006 with the FEROS spectrograph (Kaufert et al. 1999) and MPI/ESO 2.2-m telescope (Proposal ID. 77.D-0478A, PI: M.Parthasarathy). The resolving power is $R \sim 48\,000$ and the wavelength coverage is from 3600 to 9200 Å. During a 45 min exposure we achieved a signal-to-noise ratio of about 100 at the wavelength of about 5400 Å. The reduction of the FEROS spectrum was performed by the on-line software, including flat-field correction, background subtraction, removal of cosmic rays, wavelength calibration, barycentric velocity correction, and continuum normalisation. More details of instrument set up, observations and data reduction can be found in (Otsuka et al. 2017).

2.2 Low resolution spectra

Our low resolution spectroscopic observations were carried out in 11 May 2012 at the 1.9-m telescope of the South

African Astronomical Observatory (SAAO) with a long-slit spectrograph at the Cassegrain focus. The slit was $\sim 3'$ in length and $1.''5$ in width; the scale along the slit was $0.''7/\text{pixel}$. The detector was an SiTe 266 \times 1798-pixel CCD array. A 300 lines/mm grism was used in the spectral range 3500-7200 Å. The actual spectral resolution was FWHM=4.5 Å. Spectra of a Cu-Ar-filled lamp were taken to calibrate the wavelengths after each observation. Bias and flat-field images were also obtained for each night of observations to perform the standard reduction of two-dimensional spectra.

In addition, we used the spectroscopic data for Hen 3-1013 from the appendix to the "Spectroscopic atlas of post-AGB stars and planetary nebulae" by Suárez et al. (2006). The observations were carried out in Chile with a 1.5-m telescope at the La Silla Observatory of the European Southern Observatory (ESO) using the Boller-Chivens spectrograph. The formal resolution was 3.74 Å pixel. The spectrum was taken in the period March 13-17, 1994, in the spectral range 3285-10 980 Å.

3 ANALYSIS OF THE HIGH RESOLUTION SPECTRUM

3.1 Description of the spectrum

The optical spectrum of Hen 3-1013 displays stellar absorption lines and nebular emission features. The complete continuum-normalised and smoothed spectrum of Hen 3-1013 in the spectral ranges 3700–7200, 7340–7540, 7720–7920 and 8330–8530 Å is presented in Appendix A (Fig. A1). We used the adjacent averaging by 10 points to smooth the spectrum.

The search and identification of the lines in spectrum of Hen 3-1013 was carried out by using of spectral orders of echelle normalised to stellar continuum starting from 3800 to 9000 Å. The standard wavelengths of the lines were taken in the main from the tables by Moore (1945), the National Institute of Standards and Technology (NIST) Atomic Spectra Database¹ and the Fe II-data by Nave & Johansson (2012).

3.1.1 Nebular emission lines

The list of emission lines in Hen 3-1013 is given in Table 1. It includes the measured and laboratory wavelength (in the air), the equivalent width (W_{λ}), the radial velocity (V_r) with respect to Sun, the name of the element and the multiplet number to which the measured line belongs. The hydrogen lines in the table are missed owing to they have the complex multicomponent profiles and will be discussed separately.

The permitted emission lines, in addition to hydrogen, belong to the ions of Si II (from 1, 4, 5 multiplets), Mg II (7, 8, 9, 10), Fe II (38, 42, 49), Al II (3, 4, 9, 10), and also to the nonionised atoms of O I (3), N I (8).

The forbidden emission lines are represented mainly by the lines of [Fe II] from multiplets 6F, 7F, 19F, 20F, 21F and others, [Ni II] - by three lines in the red and near-infrared of 2F multiplet and in visible - from 14F multiplet. In the range of 8000-8300 Å the lines of [Cr II] of 1F multiplet are

¹ <https://www.nist.gov/pml/atomic-spectra-database>

Table 1. Emission lines in Hen 3-1013.

$\lambda_{\text{obs.}}$ (Å)	$\lambda_{\text{lab.}}$ (Å)	Identification	W_λ (Å)	V_r (km s ⁻¹)
3853.12	3853.66	Si II(1)	0.033	-42.82
3855.42	3856.00	Si II(1)	0.044	-46.68
4200.33	4200.89	Si II	0.024	-39.99
4243.47	4243.97	[Fe II](7F)	0.026	-35.32
4286.93	4287.39	[Fe II](7F)	0.076	-30.79
4358.79	4359.34	[Fe II](7F)	0.040	-37.85
4390.01	4390.58	Mg II(10)	0.022	-38.95
4413.20	4413.78	[Fe II](7F)	0.032	-39.39
4433.46	4433.99	Mg II(9)	0.019	-35.86
4457.41	4457.95	[Fe II](6F)	0.020	-36.31
4583.23	4583.83	Fe II(38)	0.025	-39.27
4813.97	4814.55	[Fe II](20F)	0.041	-36.14
4889.16	4889.63	[Fe II](3F), 4F bl	0.022	-28.84
4904.86	4905.35	[Fe II](20F)	0.017	-29.97
5040.35	5041.03	Si II(5)	0.030	-40.47
5055.27	5055.98	Si II(5)	0.043	-42.13
5158.13	5158.81	[Fe II](19F)	0.051	-39.54
5184.97	5185.56	Si II(5)	0.031	-34.13
5197.29	5197.90	[N I], Fe II(49)	0.041	-35.21
5261.02	5261.61	[Fe II](19F)	0.037	-33.64
5275.26	5275.82	[Ni II], Fe II(49)	0.021	-31.84
5465.92	5466.45	Si II	0.071	-29.09
5956.84	5957.57	Si II(4)	0.041	-36.76
5978.27	5978.93	Si II(4)	0.107	-33.12
6231.06	6231.75	Al II(10)	0.057	-33.22
6238.86	6239.60	Si II(4)	0.082	-35.58
6242.67	6243.36	Al II(10)	0.074	-33.16
6248.12	6248.91	Fe II(74)	0.022	-37.93
6317.19	6317.98	Fe II(J)	0.070	-37.51
6442.14	6442.97	Fe II(J)	0.040	-38.62
6666.04	6666.89	[Ni II](2F)	0.035	-38.25
6822.69	6823.48	Al II(9)	0.015	-34.73
6828.99	6829.83	Si II	0.021	-36.90
6836.34	6837.14	Al II(9)	0.038	-35.10
6851.01	6851.89	Fe II(J)	0.017	-38.50
7041.15	7042.06	Al II(3)	0.097	-38.77
7055.67	7056.60	Al II(3)	0.054	-39.54
7377.06	7377.83	[Ni II](2F)	0.249	-31.31
7410.75	7411.61	[Ni II](2F)	0.053	-34.81
7494.75	7495.63	Fe II(J)	0.059	-35.22
7505.70	7506.54	Fe II(J)	0.064	-33.57
7512.30	7513.18	Fe II(J)	0.154	-35.14
7730.85	7731.67	Fe II(J)	0.079	-31.80
7847.82	7848.80	Si II	0.086	-37.44
7848.78	7849.72	Si II, Fe II	0.121	-35.93
7876.02	7877.05	Mg II(8)	0.268	-39.23
7895.31	7896.37	Mg II(8)	0.409	-40.27
7999.08	8000.07	[Cr II](1F)	0.140	-37.12
8124.31	8125.30	[Cr II](1F)	0.087	-36.55
8213.11	8213.99	Mg II(7)	0.202	-32.14
8233.63	8234.64	Mg II(7)	0.265	-36.80
8286.72	8287.59	Fe II(J)	0.200	-31.49
8307.48	8308.51	[Cr II]	0.070	-37.19
8445.44	8446.25	O I	1.039	-28.77
8450.06	8451.01	Fe II(J)	0.144	-33.72
8489.13	8490.10	Fe II(J)	0.157	-34.28
8616:	8616.96	[Fe II](13F)	–	–
8628.21	8629.24	N I(8)	0.081	-35.81
8635.53	8636.58	Fe II(J)	0.075	-36.47
8639.64	8640.70	Al II(4)	0.062	-36.80
8925.81	8926.90	Fe II, Al II	0.248	-36.63

observed. The forbidden line of [N I] λ 5198 are presented. In the red and the near infrared there are seen the numerous emissions Fe II from the intercombination transitions (designated as J) whose excitation usually put down to the fluorescence due to the Ly α or to the ultraviolet continuum of the star.

We have estimated the intensities of two forbidden lines of [Ni II] from 2F multiplet in the near-IR of Hen 3-1013. Their flux ratio was found to be $I(7411)/I(7378) = 0.20 \pm 0.01$. In the pure collisional excitation this value is about 0.1 (Bautista et al. 1996) if the electron density $N_e < 10^6 \text{ cm}^{-3}$ (by $T_e \sim 10000 \text{ K}$). Lucy (1995) had studied the cause of anomalously strong emission the lines at λ 6667, 7378 and 7412 of 2F multiplet [Ni II] observable in a variety gaseous nebulae and suggested the photon pumping of these by background UV continuum. Bautista et al. (1996) have computed the line ratio $I(7411)/I(7378)$ in the three-level model of [Ni II] depending on the electron density of ambient gas and have shown that if $N_e \geq 10^7 \text{ cm}^{-3}$ the photon pumping missed. The gaseous envelope of Hen 3-1013 very probably may be the partially ionized zone (PIZ) and may have the high enough electron density ($N_e = 10^6 - 10^7 \text{ cm}^{-3}$). The reasonable difference of radial velocities found on emission and absorption lines in star spectrum allows us to assume this. The comparison of the observed line ratio (without interstellar reddening) and the theoretical one (Bautista et al. (1996), Fig.3) testified to the pure collisional excitation of [Ni II] lines in the gaseous shell of Hen 3-1013 with N_e near 10^7 cm^{-3} .

The mean radial velocities of the emission lines for various elements are shown in Table 2. In this table N designates the number of lines used to take the mean V_r . Particularly we note that the mean V_r of the emission lines in the spectrum of Hen 3-1013 are practically the same for all revealed chemical elements (except for hydrogen) and that the difference of V_r between the permitted and forbidden lines of the same element is absent.

On the whole the average heliocentric radial velocity of the emission envelope in Hen 3-1013 turned out to be $V_r = -36.0 \pm 0.4 \text{ km s}^{-1}$.

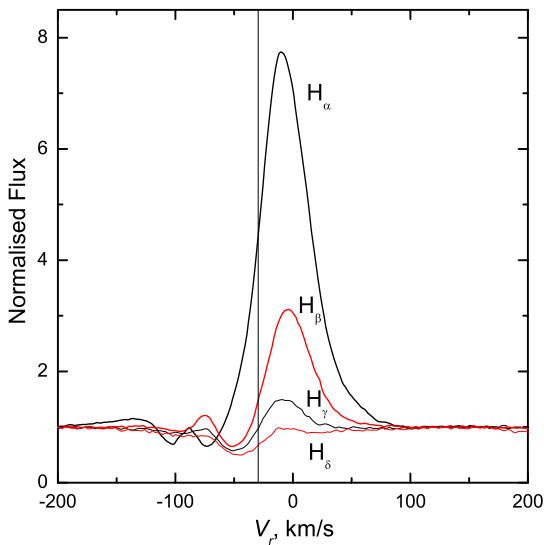
We measured nebular expansion velocity (V_{exp}) using the following relation: $V_{\text{exp}} = 1/2(V_{\text{FWHM}}^2 - V_{\text{instr}}^2)^{1/2}$, where V_{FWHM} is the velocity corresponding to the full width at half maximum (FWHM) and V_{instr} (6 km s⁻¹) is the instrumental broadenings. For the [Ni II] λ 7378 emission line V_{FWHM} equal to 25.5 km s⁻¹. The expansion velocity for Hen 3-1013 from this line is 12.4 km s⁻¹. From CO observations Loup et al. (1990) estimated expansion velocity of 15 km s⁻¹.

3.1.2 The hydrogen lines

Our material show Balmer lines from H 14 to H 7 in absorption (see Table. B1). The H α , H β and H γ lines are dominated by emission component. The H δ line is also partly contaminated by the emission component. As to emission lines of hydrogen so the profiles of H α -H δ lines are shown at Fig. 1 where the velocities are in the heliocentric frame. The strong H α emission with broad wings has $V_r = -7.8 \text{ km s}^{-1}$ and the red wing of this line extend more than 100 km/s. In the blue wing of H α there are seen two absorption components on $V_r(1) = -70 \text{ km s}^{-1}$ and $V_r(2) = -100$

Table 2. The mean heliocentric radial velocity of emission lines of selected ions in Hen 3-1013.

ion	V_r (km s $^{-1}$)	N
Fe II	-35.51 ± 0.68	14
Si II	-37.90 ± 1.39	12
Mg II	-37.18 ± 1.21	6
Al II	-35.88 ± 0.96	7
[Ni II]	-34.77 ± 2.00	3
[Fe II]	-35.42 ± 1.15	9
[Cr II]	-36.93 ± 0.20	3

**Figure 1.** Balmer lines in the spectra of Hen 3-1013. The velocities are in the heliocentric frame. The vertical line marks the radial velocity determined from absorption lines.

km s $^{-1}$. Uncertainty in the V_r is about 1 km s $^{-1}$. The other H I emissions have: $V_r(\text{H}\beta) = -7.4$ km s $^{-1}$, $V_r(\text{H}\gamma) = -9.0$ km s $^{-1}$, $V_r(\text{H}\delta) = -6.0$ km s $^{-1}$. The equivalent widths of the emission components of H α , H β are equal to 7.63 and 1.65 Å respectively.

We compared the H α profile on our spectrum and on the spectrum obtained on the same telescope with the same spectrograph in September 2007 or May 2008 (Mello et al. 2012). It should be noted that our H α profile is different from that previously reported by Mello et al. (2012). In particular, on our spectrum, the wings are narrower and there is a weak emission component at wavelength 6560.9 Å which is not in the spectrum from Mello et al. (2012).

Pashen lines on our spectrum are presented by high members from P16 and more. The line profile of each of them consist of the absorption component and more weak emission disposed on the blue wing of absorption. The mean velocity of Pashen absorptions is near Balmer emission and is about -8 km s $^{-1}$.

Table 3. The mean heliocentric radial velocity of absorption lines of selected ions in Hen 3-1013.

ion	V_r (km s $^{-1}$)	N
He I	-23.66 ± 1.29	22
O I	-31.61 ± 1.37	7
O II	-31.35 ± 0.62	48
N II	-32.17 ± 0.63	34
C II	-29.21 ± 1.44	13
S II	-25.92 ± 0.62	30
Fe II	-32.49 ± 1.34	13
Si II	-24.62 ± 1.28	6
Ar II	-33.28 ± 1.31	7
S III	-27.16 ± 1.80	7
Fe III	-29.27 ± 2.54	7
Si III	-31.24 ± 1.74	8
Si IV	-26.31 ± 0.12	2

3.1.3 Photospheric absorption lines

All of the identified absorption lines together with their radial velocity and equivalent weight are summarized in Table B1. In the column 1 the measured wavelength of the line is given, the columns 2-3 - the standard wavelength of identified ion (of the primary component if the blend) with multiplet number, the columns 4-5 - the possible member of the line if in the blend, the column 6 - the equivalent width of primary absorption line, the column 7 - the radial velocity of the single component or the primary component in the blend.

Absorption lines of neutral species including H I, He I, C I, N I, O I and Ne I were identified. Singly-ionized species including C II, N II, O II, Si II, S II, Ar II, Fe II, Mn II, Cr II, V II, Ti II, Co II, Ni II, Al II, Cu II and Cs II were detected. Higher ionization is seen in Si III, S III, Fe III and Si IV.

The mean radial velocities of the absorption lines for various elements are shown in the Table 3. The comparison of mean values V_r absorption lines of the various elements may point out on some stratification of the chemical element's velocity in the atmosphere of Hen 3-1013: for example, V_r of S II and Si II absorptions distinguish from average V_r of other absorptions so far as 5 km s $^{-1}$.

Radial velocities measured from non-blend lines are -29.6 ± 0.4 km s $^{-1}$, which is in good agreement with the previous estimate of -29.8 ± 2.1 km s $^{-1}$ (Mello et al. 2012).

3.1.4 Interstellar features and colour excess

The Na I double resonance D-lines in the high-resolution spectrum of Hen 3-1013 show a complex profiles. Four absorption components were identified in the Na I D2 and Na I D1 lines (see Fig. 2 and Table 4). The velocities of the component 2: $V_r = -37.0 \pm 0.8$ km s $^{-1}$ are comparable with the mean heliocentric radial velocity of the emission lines in the star $V_r = -36.0 \pm 0.4$ km s $^{-1}$, suggesting that this component arises in an extended envelope around the central star. We may infer that 1, 3 and 4 components in the velocity interval from -5 to -47 km s $^{-1}$ originate in the interstellar medium.

In the spectrum Hen 3-1013 we identified the most famous Diffuse Interstellar Bands (DIBs) (Hobbs et al. 2008)

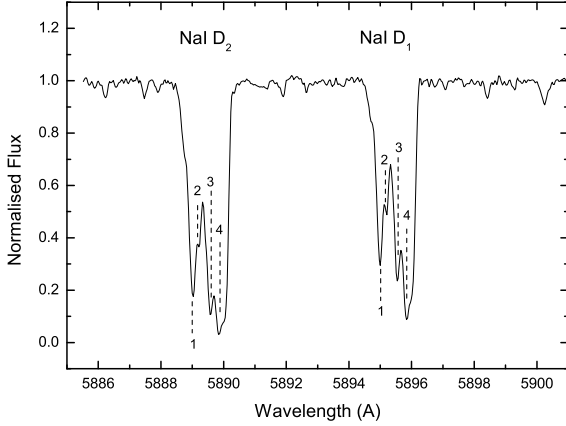


Figure 2. Na I D₂ and Na I D₁ lines in the spectra of Hen 3-1013. The various absorption components have been labelled.

Table 4. Absorption components of Na I D₂ (5889.95 Å) and Na I D₁ (5895.92 Å) lines in the spectrum of Hen 3-1013. V_r are the respective heliocentric radial velocities.

component	Na I D ₂		Na I D ₁	
	$\lambda_{\text{obs.}}$ (Å)	V_r (km s ⁻¹)	$\lambda_{\text{obs.}}$ (Å)	V_r (km s ⁻¹)
1	5889.03	-47.01	5895.00	-46.96
2	5889.21	-37.84	5895.21	-36.28
3	5889.57	-19.51	5895.54	-19.49
4	5889.84	-5.76	5895.84	-4.22

Table 5. DIBs in Hen 3-1013

$\lambda_{\text{obs.}}$ (Å)	$\lambda_{\text{lab.}}$ (Å)	FWHM (Å)	W_λ (Å)
4430.40	4428.19	1.83	-0.12
5485.20	5487.69	0.92	-0.02
5704.70	5705.08	2.81	-0.12
5780.37	5780.48	1.98	-0.22
5796.87	5797.06	0.87	-0.04
6195.80	6195.98	0.84	-0.03
6203.81	6203.05	2.14	-0.09
6269.67	6269.85	1.25	-0.04
6283.65	6283.84	5.50	-0.82
6379.05	6379.32	0.87	-0.06
6613.48	6613.62	0.97	-0.08

(see Table 5). We estimated an interstellar $E(B - V) = 0.43$ mag from the measured $W_\lambda = 0.22$ Å for the $\lambda 5780$ using the correlation W_λ with $E(B - V)$ obtained by Friedman et al. (2011).

The interstellar extinction estimate of Hen 3-1013 from the 2200 Å feature in the UV: $E(B - V) = 0.44$ mag (Gauba & Parthasarathy 2003) is in good agreement with the colour excess $E(B - V)$ was determined by us from DIB $\lambda 5780$. The total colour excess of Hen 3-1013 turned out as $E(B - V) = 0.71$ mag (Gauba & Parthasarathy 2003) hence the star have observable circumstellar extinction.

3.2 Parameters of the stellar atmosphere

To determine the main model parameters of the atmosphere, such as the effective temperature and gravity, we used non-LTE, plane-parallel, hydrostatic model atmosphere BSTAR2006 grid (Lanz & Hubeny 2007) in the TLUSTY package (Hubeny & Lanz 1995). We first estimate a surface gravity for the sample star using Balmer H 7 $\lambda 3835$. For this exercise, we adopt an initial guess of $T_{\text{eff}} = 19\,000$ K, then searched for a $\log g$ value that produce observed profile of the H 7 line. As a result of this exercise, we have obtained $\log g = 2.3$. We then, estimated T_{eff} based on Si III/Si IV ionization balance. This exercise yields $T_{\text{eff}} = 17\,750$ K. We have used Si and O absorption lines to estimate the micro-turbulent and rotational velocity. This results in $\xi_t = 24$ km s⁻¹ and $v \sin i = 5$ km s⁻¹.

The initial estimations of T_{eff} , $\log g$ and ξ_t have been iterated until a consistent set of parameters are obtained. We have finally obtained the values: $T_{\text{eff}} = 18\,250 \pm 500$ K, $\log g = 2.3 \pm 0.05$ dex, $\xi_t = 32 \pm 3$ km s⁻¹ and $v \sin i = 5 \pm 1$ km s⁻¹.

Mello et al. (2012) obtained $T_{\text{eff}} = 16\,200 \pm 300$ K, $\log g = 2.04$, $\xi_t = 17$ km s⁻¹ and $v \sin i = 38 \pm 5$ km s⁻¹. The rotational velocity obtained by them is very high and ξ_t obtained by them is low compared to the value that we obtained. This may be the reason for differences in T_{eff} values. A careful reanalysis of all the absorption line profiles is needed, which is beyond the scope and aim of the present paper. In this range of temperatures of B stars, the effects of T_{eff} and surface gravity on the wings of Hydrogen lines are degenerate: roughly similar H theoretical profiles can be computed with pairs (T_{eff} ; $\log g$) and ($T_{\text{eff}} - 1\,000$ K; $\log g - 0.1$), for example. This degeneracy, in principle, may explain the differences between the results obtained in the present paper and those published by Mello et al. (2012).

Gauba & Parthasarathy (2003) from an analysis of the UV (*IUE*) low resolution spectra derived $T_{\text{eff}} = 16\,200$ K and $\log g = 2.6$ which are in reasonable agreement with those derived by Mello et al. (2012). The T_{eff} and $\log g$ values derived from the UV flux distribution are sensitive to interstellar reddening and circumstellar reddening values.

4 LOW-RESOLUTION SPECTROSCOPY

Fig. 3 presents the low-resolution spectra of Hen 3-1013 obtained by Suárez et al. (2006) in 1994 and by us in 2012. In contrast to the high-resolution spectrum, these spectra show only the strongest lines, namely, the emission lines H α , H β , O I $\lambda 8446$, [Ni II] $\lambda 7378$ and the absorption lines O I $\lambda 7774$, the Na I D interstellar resonance lines, DIBs at $\lambda 4430$ and $\lambda 6282$. One of our interests is to check whether the spectrum has changed from 1994 to 2012.

We measured the equivalent widths of the strongest emission and absorption lines in the low-resolution spectrum of Hen 3-1013 and provide them in Table 6. The line equivalent widths in the spectrograms taken at different dates agree well between themselves. Thus, the star's spectrum underwent no significant changes from 1994 to 2012. The emissions of [Ni II] $\lambda 7378$ and H α on low-resolution spectra are stronger than in high-resolution spectra. These differences may be associated to a greater extent with the difference in spectral resolution.

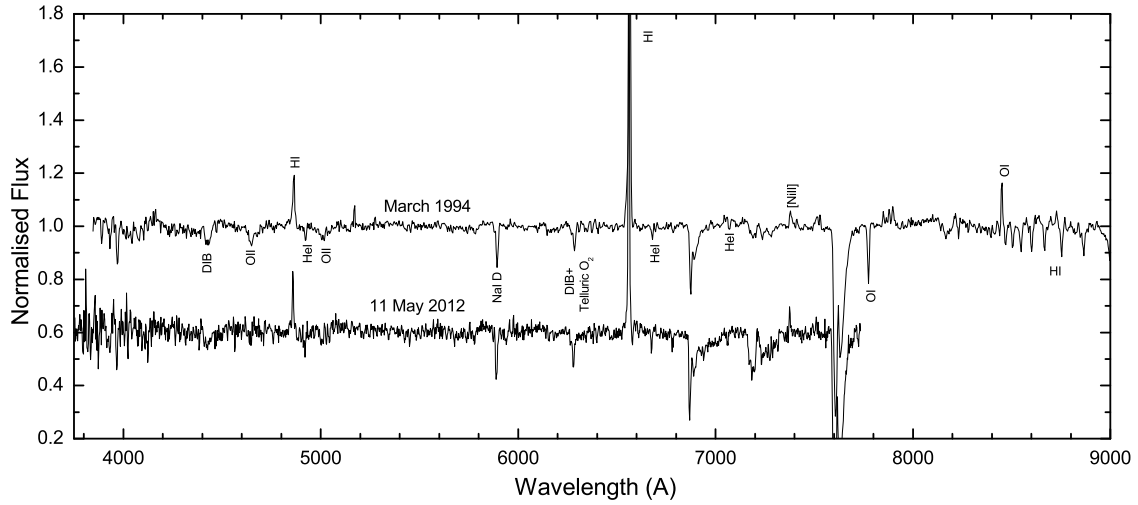


Figure 3. The low-resolution optical spectra of Hen 3-1013 from Suárez et al. (2006) (top) and obtained in SAAO (bottom) normalised to the continuum. The principal lines and most prominent DIBs are indicated. For clarity, the spectra are offset by 0.4 continuum flux unit.

Table 6. Equivalent widths of several lines in the low-resolution spectrum of Hen 3-1013.

λ (Å)	Ion	$W_\lambda \pm \sigma_{W_\lambda}$ (Å)	
		1994-03	2012-05-11
4861	H β	2.1 ± 0.2	1.8 ± 0.2
6563	H α	17.1 ± 0.6	15.0 ± 0.4
6678	He I	-0.40 ± 0.08	-0.40 ± 0.10
7378	[Ni II]	0.76 ± 0.08	0.60 ± 0.10

5 PHOTOMETRIC VARIABILITY AND HISTORY OF HEN 3-1013

Hen 3-1013 is present in the Cape Photographic Durchmusterung (CpD) (Gill & Kapteyn 1900) as CpD-64°2939 with $m_{pg} = 9.7$ mag, which allowed the photometric history of the star to be traced over more than 100 years. However, photographic magnitudes m_{pg} from the CpD catalogue should be analysed before they are compared with the present-day photometric data.

We selected 41 stars contained in the CpD from a $1^\circ \times 1^\circ$ neighbourhood of Hen 3-1013 and derived the relationship between the B magnitudes from SIMBAD and the photographic magnitudes m_{ph} from the CpD of Hen 3-1013 and stars from its neighbourhood (Fig. 4). The relationships between B and m_{pg} of the stars from the neighbourhood obey the quadratic polynomial law, according to which m_{pg} of Hen 3-1013 from the CpD is transformed into the B magnitude ~ 11.4 mag.

During 1973 and 1974 2 UBV measurements of the star were obtained by Klare and Neckel (1977). Hen 3-1013 was also observed by Kozok (1985) from 1979 (2 nights) to 1980 (3 night). According to the UBV data from Kozok (1985),

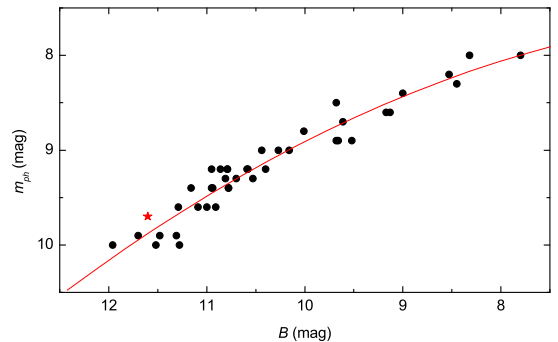


Figure 4. Relationship between the B magnitudes from SIMBAD and the photographic magnitudes from the CpD for Hen 3-1013 (asterisk) and the stars from its neighbourhood (dots). The dashed lines indicate parabola fits to the data for the stars from the neighborhoods.

the brightness Hen 3-1013 changed by 0.1 mag, with the error of a single observation being 0.010-0.015 mag.

Hen 3-1013 fell within the field of view of the All Sky Automated Survey (ASAS) (Pojmanski 2002). The observations in the ASAS-3 system have been carried out in 2001-2009 at the Las Campanas (Chile) telescopes in an automatic mode in a photometric V band close to Johnson's standard V . To analyse the ASAS-3 data, we used the measurements made with aperture 1 ($15''$) and marked in the ASAS-3 database by symbol A (good quality). The mean accuracy of the measurements was 0.04 mag.

All Sky Automated Survey for Super-Novae (ASAS-SN) is an all-sky survey that monitors the entire sky for

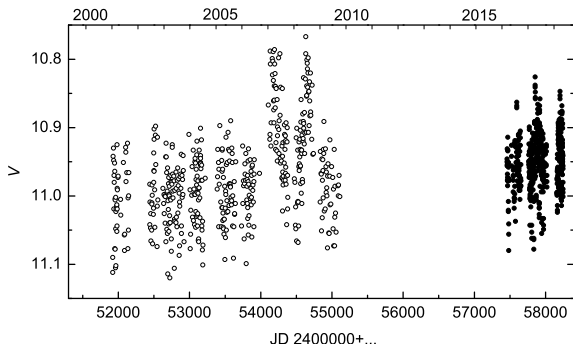


Figure 5. ASAS (the open circles) and ASAS-SN (the filled circles) V band light curve of Hen 3-1013 from 2001 to 2018

transients every night to a depth of V -band of ~ 17 mag (Shappee et al. 2014; Kochanek et al. 2017). The field containing Hen 3-1013 was observed a total of 505 times from 2016 March 10 to 2018 May 7 by bh camera in the station, located at the Cerro Tololo International Observatory (CTIO, Chile). The mean photometric uncertainty for these choices is 0.008 mag.

Fig. 5 shows the light curves derived from ASAS-3 and ASAS-SN data. The pattern of variability for Hen 3-1013 is similar in both characteristic time scales of brightness variations and oscillation amplitudes. The mean brightness in V -band from ASAS and ASAS-SN are listed in Table 7.

The star displays a brightness variation with an amplitude (peak-to-peak) of up to 0.2 mag in V -band. Light variability may be considered real since 3σ -threshold is exceeded several times.

The ASAS light curve from 2001 to 2006 and in 2009 (see Fig. 5) shows a short time-scale irregular variability with an amplitudes of 0.1-0.2 mag and roughly equal seasonal means ($V \sim 11.0$ mag).

ASAS data in 2007 display a trend of decreasing brightness. In 2008, the star’s brightness systematically increased. Superimposed on this trends is a clear fast variation with amplitude up to 0.15 mag. The mean brightness in 2007-2008 is 0.1 mag higher, when compared to the earlier and later ASAS measurements (see Table 7).

According to higher precision and better time-resolution ASAS-SN data in 2016-2018, the star brightness changes more regularly with characteristic time from 6 to 15 days in different seasons. The peak-to-peak range varies from 0.05 to 0.17 mag in V . We failed to determine the period both in the total dataset and in the subsets of single seasons. The variability of Hen 3-1013 is very similar to that of hot post-AGB star IRAS 19336-0400 (Arkhipova et al. 2012).

In Table 7, together with ASAS and ASAS-SN data, the transformed value from CpD, the average UBV magnitudes from Klare and Neckel (1977) and Kozok (1985) are listed. As can be seen from Table 7, in more than 100 years, the mean brightness of Hen 3-1013 has not changed.

Table 7. Summary of photometric observations of Hen 3-1013.

Date	U (mag)	B (mag)	V (mag)	source
before 1900	–	~ 11.4	–	(1)
1973-1974	11.128	11.485	10.889	(2)
1979-1980	11.112	11.479	10.899	(3)
2001-2006	–	–	11.00 ± 0.05	ASAS-3
2007-2008	–	–	10.91 ± 0.07	ASAS-3
2009	–	–	10.99 ± 0.05	ASAS-3
2016-2018	–	–	10.95 ± 0.04	ASAS-SN

(1) – Gill & Kapteyn (1900); (2) – Klare and Neckel (1977); (3) – Kozok (1985).

6 DISCUSSION AND CONCLUSIONS

Based on high-resolution ($R \sim 48\,000$) observations we have studied the optical spectrum of the B-supergiant Hen 3-1013, the central star of the IR-source IRAS 14331-6435. At wavelengths from 3700 to 8820 Å, numerous absorption and emission lines have been identified, their equivalent widths and corresponding radial velocities have been measured. Using non-LTE model atmospheres, we have obtained the effective temperature $T_{\text{eff}} = 18250$ K, gravity $\log g = 2.3$ and microturbulence velocity $\xi_t = 32$ km s $^{-1}$.

The presence of emission lines indicates a low-excitation nebula surrounding the B-type central star. Nebular expansion velocity (V_{exp}) is about 12 km s $^{-1}$. It is a typical value for post-AGB objects.

In the spectrum of Hen 3-1013, unlike the spectra of hotter post-AGB stars with $T_{\text{eff}} > 20\,000$ K, there are as yet no emission lines ([N II], [O II], [O III], [S II]) by which the parameters of the gas shell (T_e and N_e) could be obtained. Analysis of [Ni II] lines in the gaseous shell gives an rough estimate for the electron density $N_e \sim 10^7$ cm $^{-3}$.

It should be noted that the emission line of [Ni II] $\lambda 7378$ is clearly present, but not identified in the spectra of the hot post-AGB stars IRAS 18062+2410 (Parthasarathy et al. 2000b), IRAS 13266-5551 and IRAS 17311-4924 (Sarkar et al. 2005), IRAS 22023+5249 (Sarkar et al. 2012), IRAS 17074-1845, IRAS 17311-4924 and IRAS 18023-3409 (Arkhipova et al. 2014).

Photometric variability of Hen 3-1013 has been detected for the first time. According to the ASAS data for 2001-2009 and ASAS-SN data for 2016-2018 the object exhibited brightness variations with an amplitude of up to 0.2 mag in the V band and a time scale of several days. As some of us reported previously (Arkhipova et al. 2007, 2012, 2013, 2014), the hot post-AGB candidates also display fast irregular photometric variability with amplitudes of 0.2–0.4 mag in the V band. For some of them (except for IRAS 19200+3457 and IRAS 19336-0400) there exist spectra of high resolution that allowed to detect P Cyg profiles of He I and H I lines indicating mass loss in the stars. In the spectrum Hen 3-1013 lines H α , H β and H γ also have P Cyg profiles. It was hypothesized that an unsteady stellar wind is mainly responsible for the brightness variations.

Published results combined with our new data indicate that Hen 3-1013 is indeed in the post-AGB phase. Theoretical calculations of the post-AGB evolution of intermediate-mass stars predict comparatively short transition times of the star from an AGB giant to a hot subdwarf and then

to a white dwarf. Depending on the initial mass of the star and the history of mass loss on the AGB and post-AGB, the HR-diagram crossing time was estimated to be from 100 to several thousand years (Blöcker 1995). The modern evolution tracks computed by Miller Bertolami (2016) are at least three to ten times faster.

We estimate the mass of Hen 3-1013 using the recent post-AGB evolutionary sequences computed by Miller Bertolami (2016). The core mass $M_c \sim 0.58M_\odot$ for the stellar parameters derived here ($T_{\text{eff}}=18\,200$ K, $\log g=2.3$) and the metallicity $Z(\text{CNO})=0.016$ from Mello et al. (2012) was obtained. For this mass timescale from the moment in which $T_{\text{eff}} \sim 7000$ K ($\log T_{\text{eff}}=3.85$) to $T_{\text{eff}} \sim 18000$ K consist of ~ 100 years. Since the bolometric luminosity in the post-AGB stage is constant, the star brightness must track the change of the bolometric correction with increasing stellar temperature. According to Flower (1996), a temperature rise from 7000 to 18000 K corresponds to a change in the bolometric correction by 1.7 mag. So we could expect decreasing brightness by 1.7 mag in V , and by 1.3 mag in B .

Based on the archival and the new photometric data, we traced the photometric history of Hen 3-1013 on a timescale longer than 100 years. No significant secular changes in the star brightness have been found. Thus, we have identified the discrepancies between observation and new post-AGB models of Miller Bertolami (2016).

7 ACKNOWLEDGMENTS

This study was supported by the National Research Foundation (NRF) of the Republic of South Africa. We wish to thank the administration of the South African Astronomical Observatory for the allocation of observing time on the 1.9-m telescope and A. Tekola for the help with observations. A. Y. K. acknowledges support from the Russian Science Foundation (project no. 14-50-00043). This research has made use of the SIMBAD database, operated at CDS, Strasbourg, France, and SAO/NASA Astrophysics Data System.

REFERENCES

- Arkhipova V.P., Ikonnikova N.P., Komissarova G.V., Noskova R.I., Esipov V.F., 2004, *Astronomy Letters*, 30, 778
- Arkhipova V. P., Esipov V. F., Ikonnikova N. P., Komissarova G. V., Noskova R. I., 2007, *Astronomy Letters*, 33, 604
- Arkhipova V.P., Burlak M.A., Esipov V.F., Ikonnikova N.P., Komissarova G.V., 2012, *Astronomy Letters*, 38, 157
- Arkhipova V.P., Burlak M.A., Esipov V.F., Ikonnikova N.P., Komissarova G.V., 2013, *Astronomy Letters*, 39, 619
- Arkhipova V.P., Burlak M.A., Esipov V.F., Ikonnikova N.P., Kniazev A.Yu., Komissarova G.V., Tekola A., 2014, *Astronomy Letters*, 40, 485
- Bautista M.A., Peng J., Pradhan A.K., 1996, *ApJ*, 460, 372
- Blöcker T., 1995, *A&A*, 299, 755
- Friedman S. D. et al., 2011, *ApJ*, 727, 33
- García-Hernández D.A., Manchado A., García-Lario P., Domínguez-Tagle C., Conway G.M., and Prada F., 2002, *A&A*, 387, 955
- Gauba G., Parthasarathy M., 2003, *A&A*, 407, 1007
- Gauba G., Parthasarathy M., 2004, *A&A*, 417, 201
- Gill D., Kapteyn J. C., 1900, *Cape Photographic Durchmusterung, Part III*
- Flower P.J., 1996, *ApJ*, 469, 355
- Henize K.G., 1976, *ApJS*, 30, 491
- Hobbs L.M., York D.G., Snow T.P., Oka T., Thorburn J.A., Bishof M., Friedman S.D., McCall B.J., Rachford B., Sonnenstrucker P., Welty D.E., 2008, *ApJ*, 680, 1256
- Hubeny I. & Lanz T., 1995, *ApJ*, 439, 875
- Kaufer A., Stahl O., Tubessing S. et al., 1999, *The Messenger*, 95, 8
- Klare G., Neckel T., 1977, *A&AS*, 27, 215
- Kochanek C.S., Shappee B.J., Stanek K.Z., Hololien T.W.-S., Thompson, Todd A. et al., 2017, *PASP*, 129:104502
- Kozak J.R., 1985, *A&AS*, 61, 387
- Lanz T. & Hubeny I., 2007, *ApJS*, 169, 83
- Loup C., Forveille T., Nyman L. A., Omont A., 1990, *A&A*, 227, L29
- Lucy L.B., 1995, *A&A*, 294, 555
- Mello D.R.C., Daflon S., Pereira C.B., and Hubeny I., 2012, *A&A*, 543, A11
- Miller Bertolami M.M., 2016, *A&A*, 588, A25
- Moore C. E., 1945, *A Multiplet Table of Astrophysical Interest*. Princeton Univ. Observatory, Princeton
- Nave G. and Johansson S. (arXiv:1210.4773v1, 2012)
- Parthasarathy M., Pottasch S.R., 1989, *A&A*, 225, 521
- Parthasarathy M., Vijapurkar J., and Drilling J.S., 2000a, *A&AS*, 145, 269
- Parthasarathy M., García-Lario P., Sivarani T., Manchado A., and Sanz Fernández de Córdoba L., 2000b, *A&A*, 357, 241
- Pojmanski G., 2002, *Acta Astronomica*, 52, 397
- Sarkar G., Parthasarathy M., and Reddy B.E., 2005, *A&A*, 431, 1007
- Sarkar G., García-Hernández D.A., Parthasarathy, Manchado A., García-Lario P., and Takeda Y., 2012, *MNRAS*, 421, 679
- Shappee B.J., Prieto J.L., Grupe D., Kochanek C.S., Stanek K. Z., De Rosa G., 2014, *ApJ*, 788:48
- Suárez O., García-Lario P., Manchado A., Manteiga M., Ulla A. and Pottasch S.R., 2006, *A&A*, 458, 173
- Otsuka M., Parthasarathy M., Tajitsu A., Hubrig S., 2017, *ApJ*, 838:71

**APPENDIX A: HIGH-RESOLUTION OPTICAL
SPECTRUM OF HEN 3-1013**

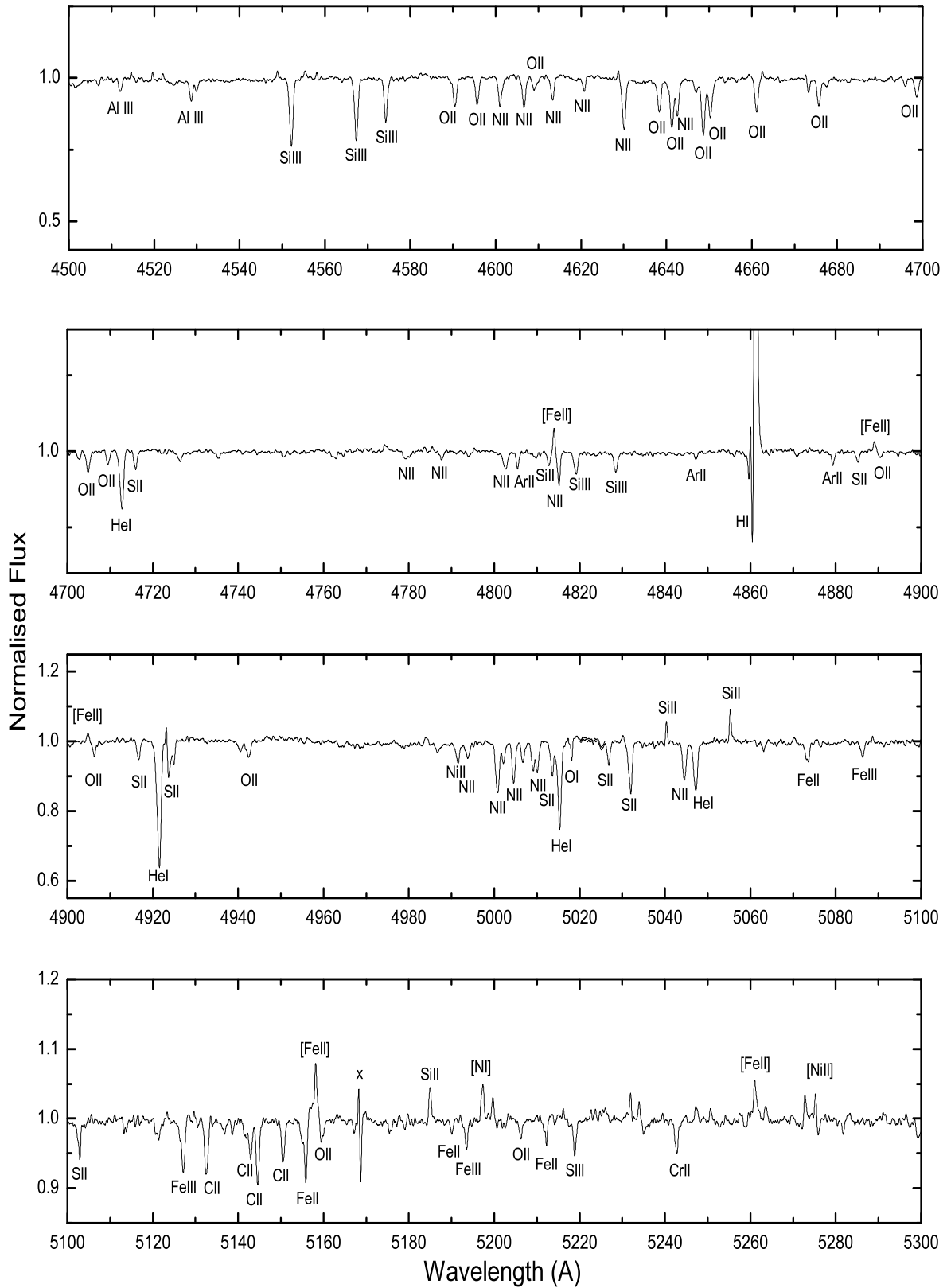


Figure A2. Optical spectrum of Hen 3-1013.

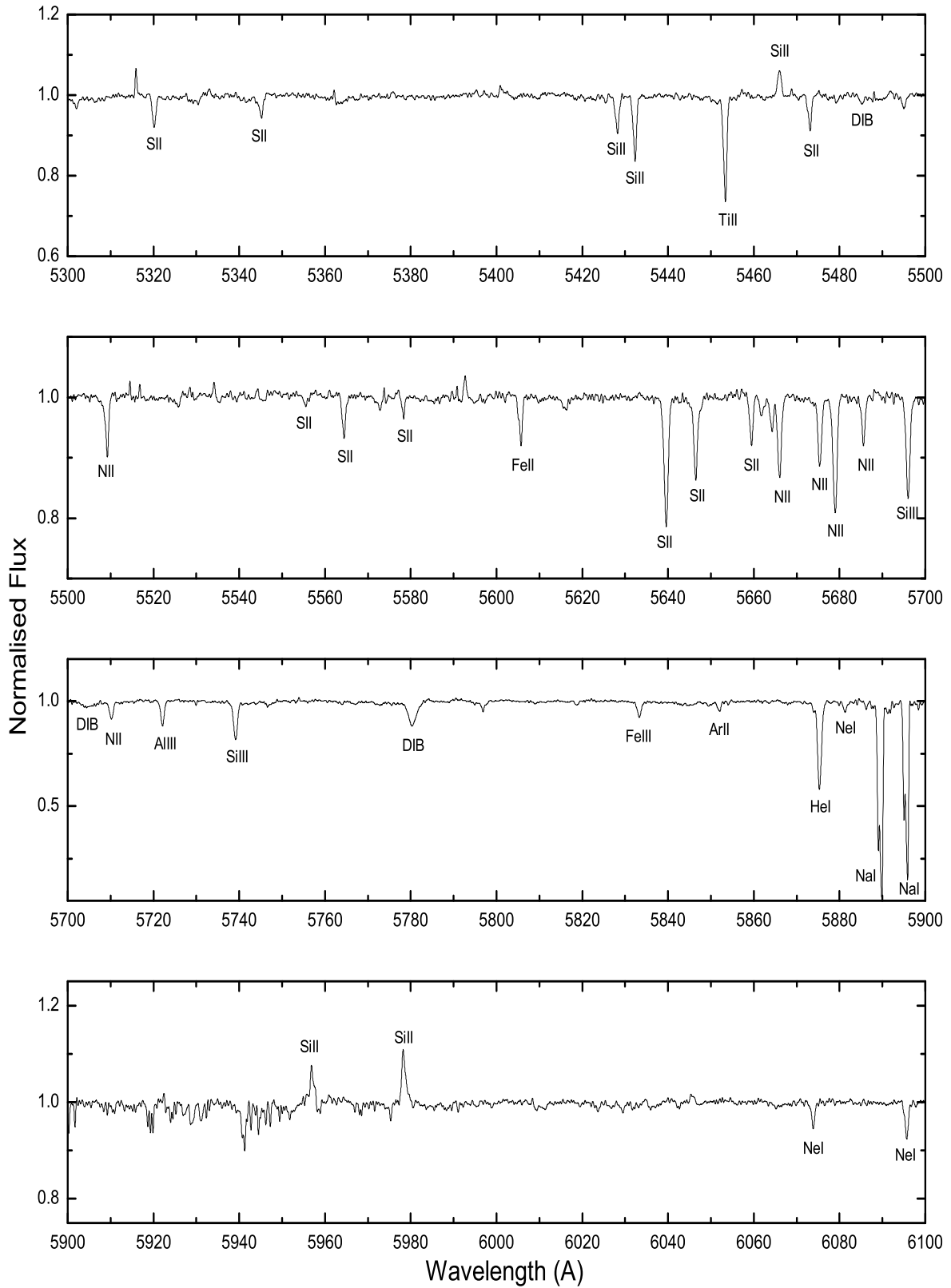
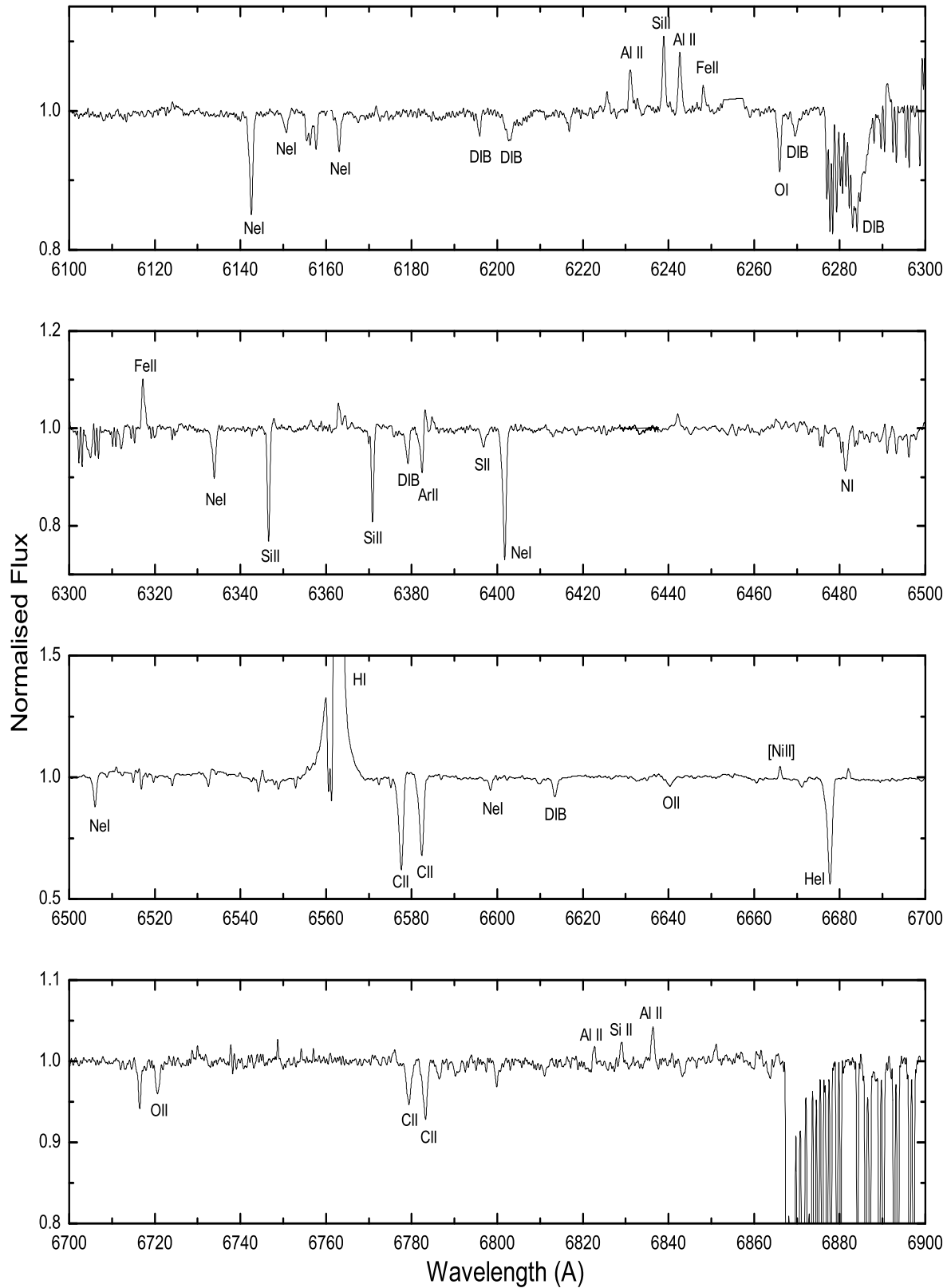


Figure A3. Optical spectrum of Hen 3-1013.



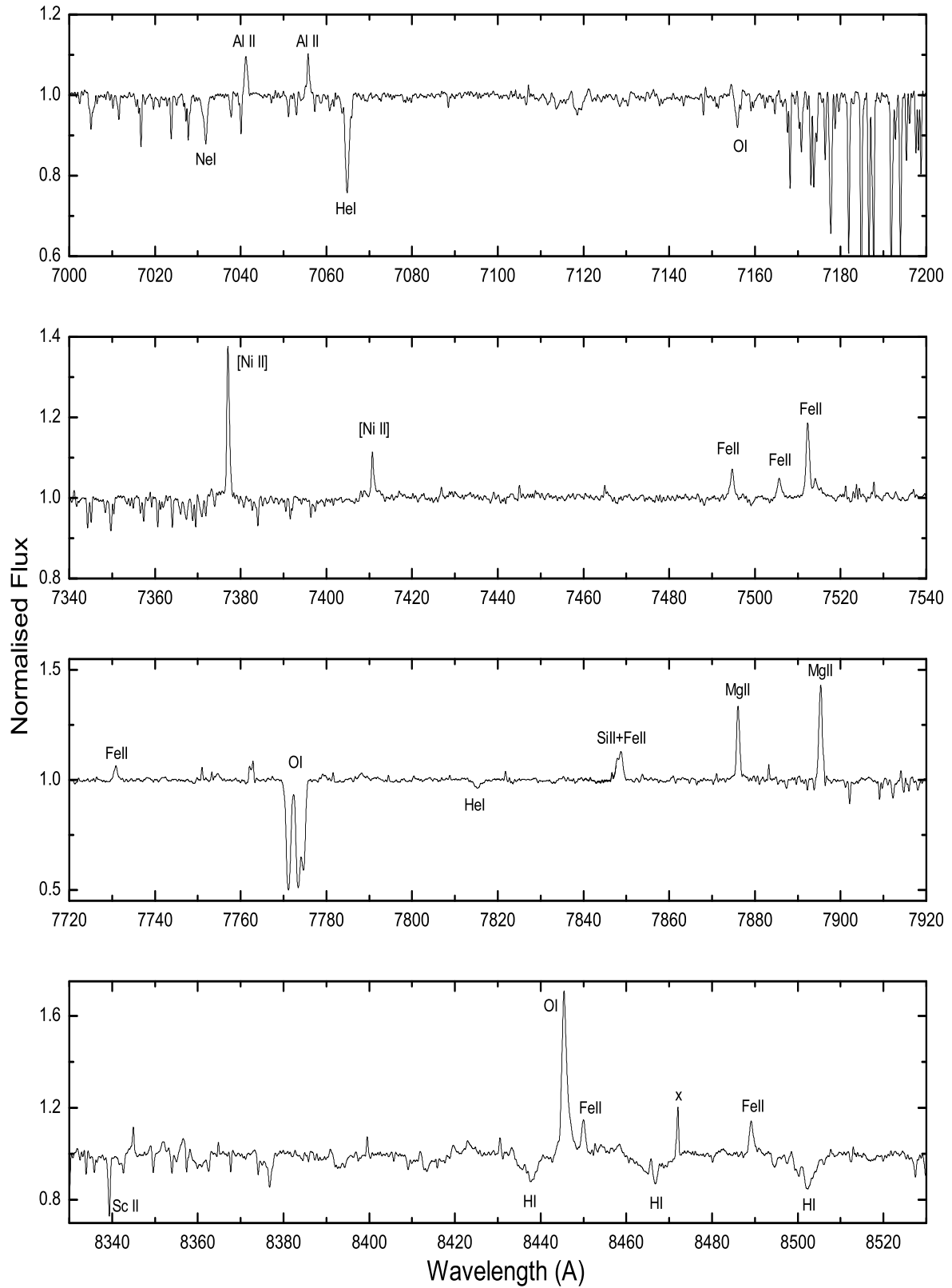


Figure A5. Optical spectrum of Hen 3-1013.

APPENDIX B: ABSORPTION LINES IN HEN 3-1013

Table B1: Absorption lines in Hen 3-1013

$\lambda_{\text{obs.}}$ (Å)	$\lambda_{\text{lab.}}$ (Å)	Ident.	W_{λ} (Å)	V_r (km s ⁻¹)
3717.42	3717.72	S III(6)	0.164	-24.19
3721.65	3721.94	H 14	0.640	-23.36
3733.88	3734.37	H 13	0.796	-39.34
3749.85	3750.15	H 12	0.708	-23.98
3770.15	3770.63	H 11	0.802	-38.16
3797.42	3797.90	H 10	0.609	-37.89
3805.94	3806.25	Ne II	0.217	-24.42
3819.30	3819.61	He I(22)	0.310	-24.33
3835.00	3835.40	H 9	0.652	-31.27
3837.84	3838.28	S III(5)	0.121	-34.37
3864.00	3864.43	O II(12)	0.054	-33.36
3871.35	3871.79	He I(60)	0.166	-34.07
3875.84	3876.19	C II(33)	0.072	-27.07
3881.90	3882.20	O II(12)	0.078	-23.17
3888.55	3889.06	H 8	0.551	-39.31
3911.56	3911.96	O II(17)	0.072	-30.65
3924.14	3924.64	N II	0.083	-38.19
3926.14	3926.53	He I(58)	0.150	-29.78
3928.14	3928.54	S III(8)	0.042	-30.52
3933.20	3933.66	Ca II(1)	0.745	-35.06
3953.85	3954.36	O II(6)	0.059	-38.66
3955.47	3955.85	N II(6)	0.091	-28.80
3964.32	3964.73	He I(5)	0.238	-31.00
3968.22	3968.72	Fe III(120)	0.635	-37.77
3969.51	3970.04	H 7	0.626	-40.02
3972.80	3973.26	O II(6)	0.164	-34.71
3982.27	3982.72	O II(6)	0.063	-33.87
3994.56	3995.00	N II(12)	0.170	-33.02
4008.97	4009.51	He I(55)	0.190	-22.43
4025.99	4026.19	He I(18)	0.374	-14.89
4040.84	4041.31	O II(50)	0.064	-34.87
4069.38	4069.89	O II(10)	0.131	-37.57
4071.86	4072.38	Ar II(41)	0.148	-38.28
4075.41	4075.94	Fe II(21)	0.136	-38.98
4078.44	4078.86	O II(10)	0.040	-30.87
4084.69	4085.12	O II(10)	0.061	-31.56
4086.81	4087.27	Fe II(28)	0.033	-33.74
4088.50	4088.86	Si IV(19)	0.090	-26.39
4092.56	4092.93	O II(10)	0.034	-27.10
4096.74	4097.26	O II(20)	0.036	-38.05
4101.13	4101.74	H 6	0.379	-44.58
4104.47	4105.00	O II(20)	0.089	-38.71
4115.74	4116.10	Si IV(1)	0.043	-26.22
4118.74	4119.22	O II(20)	0.100	-34.93
4120.42	4120.82	He I(16)	0.247	-29.10
4127.77	4128.07	Si II(3)	0.123	-21.79
4130.58	4130.89	Si II(3)	0.123	-22.50
4132.43	4132.80	O II(19)	0.073	-26.84
4143.42	4143.76	He I(53)	0.287	-24.60
4152.70	4153.06	S II(44)	0.102	-25.99
4162.19	4162.67	S II(44)	0.056	-34.57
4164.37	4164.81	Ne I	0.050	-31.67
4168.61	4168.97	He I(52)	0.060	-25.89
4189.35	4189.71	S II(44)	0.069	-25.76
4221.84	4222.27	Fe III	0.040	-30.53
4227.38	4227.749	N II(33)	0.056	-26.26

continued Table B1

$\lambda_{\text{obs.}}$ (Å)	$\lambda_{\text{lab.}}$ (Å)	Ident.	W_{λ} (Å)	V_r (km s ⁻¹)
4236.54	4236.99	N II(48)	0.065	-31.84
4241.33	4241.78	N II(48)	0.075	-31.80
4253.20	4253.50	S III(4)	0.099	-21.14
4266.78	4267.26	C II(6)	0.249	-33.72
4284.56	4284.88	S III(4)	0.084	-22.39
4294.14	4294.40	S II(49)	0.042	-18.15
4316.70	4317.14	O II(2)	0.099	-30.55
4319.10	4319.63	O II(2)	0.115	-36.78
4325.29	4325.76	O II(2)	0.032	-32.57
4332.26	4332.71	O II(65)	0.043	-31.14
4336.44	4336.86	O II(2)	0.072	-29.03
4345.11	4345.56	O II(2)	0.105	-31.04
4347.29	4347.82	Al II(70)	0.126	-36.54
4348.93	4349.43	O II(2)	0.167	-34.46
4350.74	4351.27	O II(16)	0.056	-36.52
4354.08	4354.49	S III(7)	0.027	-28.25
4361.05	4361.59	Fe II	0.048	-37.12
4366.44	4366.90	O II(2)	0.112	-31.58
4387.54	4387.93	He I(51)	0.317	-26.65
4395.53	4395.95	O II(26)	0.046	-28.64
4410.85	4411.20	C II(39)	0.032	-23.79
4414.47	4414.91	O II(5)	0.122	-29.88
4419.33	4419.78	Cr II	0.070	-30.52
4437.15	4437.55	He I(50)	0.087	-27.02
4446.53	4447.03	N II(15)	0.076	-33.71
4451.98	4452.38	O II(5)	0.028	-26.87
4471.17	4471.48	He I(14)	0.327	-20.78
4480.91	4481.21	Mg II(4)	0.255	-20.07
4512.08	4512.56	Al III(3)	0.047	-31.89
4528.57	4529.16	Al III(3)	0.064	-39.05
4552.14	4552.62	Si III(2)	0.246	-31.61
4567.42	4567.82	Si III(2)	0.213	-26.25
4574.25	4574.76	Si III(2)	0.137	-33.42
4590.42	4590.97	O II(15)	0.115	-35.92
4595.76	4596.17	O II(15)	0.099	-26.74
4601.00	4601.48	N II(5)	0.111	-31.27
4606.63	4607.16	N II(15)	0.112	-34.49
4608.99	4609.44	O II(93)	0.075	-29.27
4613.41	4613.87	N II(5)	0.091	-29.89
4620.94	4621.39	N II(5)	0.053	-29.19
4630.03	4630.54	N II(5)	0.173	-33.02
4638.39	4638.86	O II(1)	0.112	-30.37
4641.30	4641.81	O II(1)	0.187	-32.94
4642.66	4643.08	N II(5)	0.125	-27.12
4648.66	4649.13	O II(1)	0.209	-30.31
4650.34	4650.84	O II(1)	0.155	-32.23
4661.15	4661.64	O II(1)	0.119	-31.51
4673.35	4673.73	O II(1)	0.035	-24.37
4675.68	4676.24	O II(1)	0.099	-35.90
4695.96	4696.36	O II(8)	0.016	-25.53
4698.62	4699.21	O II(25)	0.067	-37.64
4704.80	4705.36	O II(25)	0.074	-35.68
4709.45	4710.00	O II(24)	0.046	-35.01
4712.84	4713.14	He I(12)	0.203	-19.08
4715.95	4716.27	S II(9)	0.059	-20.34
4779.11	4779.71	N II(20)	0.044	-37.63
4787.66	4788.13	N II(20)	0.028	-29.43
4802.68	4803.27	N II(20)	0.068	-36.82
4805.43	4806.02	Ar II(6)	0.041	-36.80

continued Table B1

$\lambda_{\text{obs.}}$ (Å)	$\lambda_{\text{lab.}}$ (Å)	Ident.	W_{λ} (Å)	V_r (km s ⁻¹)
4812.82	4813.33	Si III(9)	0.033	-31.76
4815.24	4815.62	N II(20)	0.078	-23.66
4819.26	4819.72	Si III(9)	0.073	-28.61
4828.38	4828.96	Si III(9)	0.063	-36.01
4847.27	4847.81	Ar II(6)	0.019	-33.39
4859.70	4860.20	Cr II(30)	0.047	-30.84
4879.34	4879.86	Ar II(14)	0.047	-31.95
4885.23	4885.65	S II(15)	0.046	-25.77
4890.50	4890.93	O II(28)	0.016	-26.36
4906.42	4906.83	O II(28)	0.047	-25.05
4916.72	4917.21	S II(15)	0.058	-29.87
4921.56	4921.93	He I(48)	0.394	-22.54
4923.69	4924.12	S II(7)	0.096	-26.18
4940.65	4941.12	O II(33)	0.050	-28.52
4986.71	4987.27	Fe II	0.032	-33.66
4991.56	4991.97	S II(7)	0.061	-24.62
4993.83	4994.36	N II(24)	0.054	-31.81
5000.94	5001.46	N II(19)	0.144	-31.17
5002.12	5002.69	N II(4)	0.054	-34.16
5004.67	5005.14	N II(19)	0.102	-28.15
5006.74	5007.32	N II(24)	0.055	-34.73
5009.12	5009.56	S II(7)	0.094	-26.33
5010.03	5010.62	N II(4)	0.084	-35.30
5013.57	5014.03	S II(15)	0.049	-27.50
5015.30	5015.68	He I(4)	0.215	-22.71
5018.21	5018.78	O I(13)	0.027	-34.05
5026.81	5027.22	S II(1)	0.043	-24.45
5031.99	5032.45	S II(7)	0.141	-27.40
5044.47	5045.10	N II(4)	0.100	-37.44
5047.22	5047.74	He I(47)	0.143	-30.88
5073.51	5074.06	Fe II(205)	0.059	-32.50
5086.31	5086.72	Fe III(5)	0.042	-24.16
5102.86	5103.34	S II(7)	0.037	-28.20
5127.12	5127.50	Fe III(5)	0.080	-22.22
5132.58	5133.10	C II(16)	0.079	-30.37
5142.85	5143.49	C II(16)	0.047	-37.30
5144.66	5145.16	C II(16)	0.075	-29.13
5150.39	5151.08	C II(16)	0.055	-32.01
5155.85	5156.45	Fe II	0.078	-34.88
5159.50	5159.94	O II(32)	0.033	-25.56
5190.19	5190.74	Fe II	0.013	-31.77
5193.52	5193.91	Fe III(5)	0.029	-22.51
5206.24	5206.65	O II(32)	0.022	-23.61
5212.30	5212.83	Fe II	0.024	-30.48
5218.81	5219.32	S III	0.039	-29.29
5242.82	5243.46	Cr II(38)	0.053	-36.59
5302.18	5302.86	Si III	0.012	-38.44
5320.20	5320.73	S II(38)	0.075	-29.86
5345.16	5345.72	S II(38)	0.049	-31.41
5428.20	5428.67	S II(6)	0.086	-25.96
5432.31	5432.82	Si II(6)	0.146	-28.14
5453.47	5454.05	Ti II	0.231	-31.88
5473.21	5473.62	S II(6)	0.079	-22.46
5495.03	5495.67	N II(29)	0.036	-34.91
5509.27	5509.72	S II(6)	0.077	-24.49
5555.56	5556.01	S II(6)	0.024	-24.28
5564.49	5564.94	S II(6)	0.068	-24.24
5578.44	5578.89	S II(11)	0.020	-24.18
5605.82	5606.37	Fe II	0.076	-29.431

continued Table B1

$\lambda_{\text{obs.}}$ (Å)	$\lambda_{\text{lab.}}$ (Å)	Ident.	W_{λ} (Å)	V_r (km s ⁻¹)
5639.58	5639.96	S II(14)	0.238	-20.20
5646.55	5647.02	S II(14)	0.141	-24.95
5659.42	5659.98	S II(11)	0.072	-29.66
5661.79	5662.47	C II(15)	0.032	-36.00
5664.31	5664.77	S II(11)	0.059	-24.34
5666.08	5666.63	N II(3)	0.142	-29.10
5675.30	5676.02	N II(3)	0.123	-38.03
5678.99	5679.56	N II(3)	0.218	-30.09
5685.58	5686.21	N II(3)	0.073	-33.22
5695.94	5696.49	Si III	0.181	-28.95
5710.20	5710.76	N II(3)	0.078	-29.40
5722.17	5722.73	Al III(2)	0.111	-29.34
5739.28	5739.73	Si III(4)	0.197	-23.50
5818.69	5819.27	S II(14)	0.018	-29.36
5833.23	5833.93	Fe III(114)	0.087	-35.97
5852.14	5852.74	Ar II	0.034	-30.73
5875.30	5875.62	He I(11)	0.456	-16.33
5881.39	5881.90	Ne I(1)	0.053	-25.99
5927.07	5927.81	N II(28)	0.024	-37.42
5929.04	5929.69	Fe III(114)	0.053	-32.86
5931.16	5931.78	N II(28)	0.034	-31.33
5951.84	5952.39	N II(28)	0.023	-27.70
5975.29	5975.96	Ar II	0.027	-33.61
6073.84	6074.34	Ne I(3)	0.048	-24.68
6095.65	6096.16	Ne I	0.067	-25.08
6142.52	6143.06	Ne I(1)	0.137	-26.35
6163.04	6163.59	Ne I(5)	0.055	-26.75
6266.09	6266.89	O I(48)	0.061	-38.27
6304.90	6305.48	S II(19)	0.077	-27.58
6312.17	6312.68	S II(26)	0.040	-24.22
6333.91	6334.43	Ne I(1)	0.092	-24.61
6346.64	6347.10	Si II(2)	0.166	-21.73
6370.83	6371.36	Si II(2)	0.128	-24.94
6382.50	6383.10	Ar II	0.076	-28.18
6396.82	6397.36	S II(19)	0.043	-25.31
6401.78	6402.25	Ne I(1)	0.257	-22.01
6481.17	6481.71	N I(21)	0.094	-24.98
6506.06	6506.53	Ne I(3)	0.117	-21.66
6532.26	6533.00	N II(45)	0.045	-33.96
6577.59	6578.03	C II(2)	0.474	-20.05
6582.33	6582.88	C II(2)	0.405	-25.05
6598.39	6598.95	Ne I(6)	0.033	-25.44
6640.46	6641.04	O II(4)	0.066	-26.18
6677.81	6678.15	He I(46)	0.571	-15.26
6720.66	6721.38	O II(4)	0.044	-32.11
6779.42	6779.94	C II(14)	0.082	-22.99
6783.20	6783.90	C II(14)	0.103	-30.93
6786.50	6787.21	C II(14)	0.044	-31.36
7031.61	7032.41	Ne I(1)	0.116	-34.10
7064.92	7065.19	He I(10)	0.247	-11.46
7156.00	7156.70	O I(38)	0.134	-29.32
7280.93	7281.35	He I(45)	0.301	-17.29
7771.15	7771.94	O I(1)	0.670	-30.32
7773.47	7774.17	O I(1)	0.691	-26.96
7774.58	7775.39	O I(1)	0.517	-31.12
7815.23	7816.10	Cr II(69)	0.074	-33.22
7963.44	7964.15	Fe II	0.050	-26.73
8007.78	8008.65	Fe II	0.045	-32.57
8205.07	8206.04	Ne II	0.019	-35.44

continued Table B1

$\lambda_{\text{obs.}}$ (\AA)	$\lambda_{\text{lab.}}$ (\AA)	Ident.	W_{λ} (\AA)	V_r (km s^{-1})
8209.94	8210.53	Fe II	0.101	-21.54
8215.69	8216.34	NI(2)	0.033	-23.72
8218.48	8219.04	Fe II	0.140	-20.44
8300.75	8301.56	Ne I	0.123	-29.25
8304.63	8305.71	Fe II	0.083	-38.98
8334.03	8335.04	Sc II	0.029	-36.18
8339.34	8340.35	Sc II	0.142	-36.30
8362.65	8363.47	Al II(40)	0.026	-29.39
8494.52	8495.36	Ne I(18)	0.068	-29.64
8581.89	8582.61	He I	0.295	-25.15
8775.85	8776.71	He I	0.215	-29.38
8819.51	8820.43	O I(37)	0.150	-31.27